INTERNATIONAL JOURNAL FOR NUMERICAL METHODS IN FLUIDS
Int. J. Numer. Meth. Fluids 2004; **44**:175–196 (DOI: 10.1002/fld.634)

Implementation and validation of a slender vortex filament code[‡]: Its application to the study of a four-vortex wake model

D. Margerit, P. Brancher[*,†] and A. Giovannini

IMFT, Allée du professeur Camille Soula, 31400 Toulouse, France

SUMMARY

A computational code EZ-vortex is developed for the motion of slender vortex filaments of closed or open shape. The integro-differential equations governing the motion of the vortex centrelines are either the Callegari and Ting equations, which are the leading order solution of a matched asymptotic analysis, or equivalent forms of these equations. They include large axial velocity and nonsimilar profiles in the vortical cores. The fluid may be viscous or inviscid. This code is validated both against known solutions of these equations and results from linear stability analyses. The linear and non-linear stages of a perturbed two-vortex wake and of a four-vortex wake model are then computed. Copyright © 2004 John Wiley & Sons, Ltd.

KEY WORDS: vortex filament; vortex method; open filament; Crow instability; aircraft wake

1. INTRODUCTION

The vortical topology of many flows consists of *several vortex filaments* submerged in a background potential flow. The two-vortex aircraft wake is an important example of these flows as it is of industrial interest. The potential hazard related to these coherent vortices induces separation distances between aircrafts and associated delay at landing and take-off, which contributes to the congestion of airports [1].

Vortex methods [2] are numerical methods of great interest to study *vortical flows*. The discretization is of the vorticity field, rather than the velocity field, and is Lagrangian in nature. It consists of a collection of particles (vortex particle methods [VP]) or filaments (vortex filament methods [VF]) which carry concentrations of vorticity. The velocity field is recovered from the discretized vorticity field via the Biot–Savart law and a *numerical*

*Correspondence to: P. Brancher, IMFT, Allée du Prof. Camille Soula, 31400 Toulouse, France.
†E-mail: brancher@imft.fr
‡The code `EZ-vortex` is available on the web or on request by email

Contract/grant sponsor: C-Wake; contract/grant number: GRD1-1999-10332

Received 1 February 2002
Revised 18 August 2003

smoothing parameter is introduced to desingularize the Biot–Savart line-integral kernel. The vorticity field is then evolved in time according to this velocity field.

The present paper focuses on the implementation of a vortex filament method adapted to solve vortical flows composed of several thin vortex filaments. This method called *slender vortex filament methods* [SVF] is based on the equation of motion obtained from an asymptotic expansion of the Navier–Stokes equations in terms of the small thickness of these vortices. The implemented code EZ-vortex provides a useful and fast tool for the simulation of aircraft wakes.

Let us recall that the induced velocity of a curved vortex filament of zero thickness, i.e. a line vortex, near its centreline is known to have a binormal component proportional to its curvature and to the logarithm of the distance to the centreline [3, 4]. The induced velocity on the centreline is thus infinite and this line vortex model is not the leading-order part of the expansion of a *slender* vortex filament in terms of its thickness. From the point of view of perturbation methods the *slender* filament corresponds to a boundary layer near its moving centreline. The original Navier–Stokes equations are then stiff to be solved numerically. By using a matched asymptotic expansion in terms of the filament thickness Callegari and Ting [5–7] have derived an equation of motion for the centreline from the Navier–Stokes equations. SVF are numerical methods which are based on the numerical discretization of this equation [8]. These methods may be inviscid or viscous and have the advantage to be rigorously derived from the Navier–Stokes equations. The thickness of the filaments has to be small compared to other characteristic length scales. Therefore they do not take into account short waves along the filament, the distance between two filaments has to be greater than their thickness, and so these methods do not allow reconnection of vorticity.

Previous to this matched asymptotic derivation several *ad hoc* desingularizations of the Biot–Savart self-induction of a line vortex were proposed [9]. These methods introduce an *ad hoc parameter of desingularization* to take care of the finite thickness of the filament. In *the cut-off method* [10, 11] the desingularization is obtained by cutting a neighbourhood of the induced velocity point in the Biot–Savart self-induction of a line vortex: the introduced *cut-off length* is the *ad hoc* parameter of desingularization. This cut-off method was used in most stability studies of slender vortex filaments [10, 12]. By a direct comparison between such *ad hoc* equations of motion and asymptotic equation of motion Widnall *et al.* [13, 14] and then Moore and Saffman [15, 4] give the relation between the cut-off length and the inner structure of the filament. More recently Margerit *et al.* [16] did the comparison with the Callegari and Ting equation. With this relation the cut-off line-integral equation of the centreline is equivalent to Callegari and Ting equation. This comparison can be done with other *ad hoc* desingularization methods. The numerical discretization of these equations gives other slender vortex filament methods. However, the resulting justified desingularization methods are still stiff to be solved numerically as the Biot–Savart desingularized integral of these methods is a singular integral in the parameter of desingularization: the centreline in the neighbourhood of any point on the filament is a boundary layer for the induced velocity contribution at this point and so needs extra discretized elements.

By using the Callegari and Ting equation Klein and Knio [17] have shown that it is not correct to compute a vortical flows composed of several thin vortex filaments by a standard VF method [2] with only one *numerical filament* per section of vortex (the so-called thin-tube model): more than one numerical filament per section is needed to insure the convergence of the numerical scheme. However, as it would save computation time to have only one

numerical filament per section Klein and Knio [17] proposed a cure: they have shown how to adjust the numerical desingularization parameter (the so-called thin-tube thickness) to physical thickness of the slender vortex filaments so that the method is correct. This corrected method is based on a comparison with the Callegari and Ting equation of motion and gives another slender vortex filament method. As for the justified desingularization methods and for the same reason, the resulting corrected thin-tube model is still stiff to be solved numerically. This stiffness of the corrected method is now removed in the *improved thin tube models* proposed by Knio and Klein [18].

In Section 2 of this paper, we give the governing equations that we have implemented in the slender vortex filament code EZ-Vortex for closed or open filaments. We first give the Callegari and Ting equation and the associated core-structure functions. We then successively give the local induction approximation (LIA) for its historical interest, a simple de-singularized method and the M1 de-singularized method of Knio and Klein. The numerical schemes used to discretize such equations and implementation issues such as the storage of filament are discussed in Section 3. In Section 4 the code is validated against exact solutions of the equations and against results of linear stability studies. The code is then used in Section 5 to study the linear and non-linear stages of a perturbed two-vortex wake and in Section 6 of a perturbed four-vortex wake. The linear stages are compared to known stability results. In Section 7 we summarize the results and give some concluding remarks.

2. THE GOVERNING EQUATIONS

In this section we give the integro-differential equations governing the motion of the centreline that we have implemented in the EZ-vortex code. They are either the Callegari and Ting equations, which are the leading order solution of a matched asymptotic analysis [6], or a simple de-singularized method, or the M1 de-singularized method of Knio and Klein [17, 18]. Even if these equations are equivalent their discretized form may be more or less advantageous from the point of view of their numerical stability or of the simplicity of their implementation as shown in Section 3. For its historical interest the local induction model (LIA) has also been implemented even if it is not equivalent to the previous equations.

2.1. The Callegari and Ting equation of a closed filament

The centreline $\mathbf{X}(s,t)$ of the filament at time t is parametrized by $s \in [-\pi, \pi[$ (see Figure 1). For each point on the centreline the Frenet frame $(\mathbf{t}, \mathbf{n}, \mathbf{b})$ is defined with, respectively, the unit tangent, normal and binormal vectors to $\mathbf{X}(s,t)$. The Callegari and Ting equation is [6]

$$\partial \mathbf{X}/\partial t = \frac{\Gamma K(s,t)}{4\pi}[-\log \varepsilon + \log(S) - 1 + C_v(t) + C_w(t)]\mathbf{b}(s,t) + \mathbf{A}(s,t) \tag{1}$$

where Γ is its circulation and K is the local curvature. The small parameter ε is the asymptotic parameter of the expansion and corresponds to the aspect ratio δ/L, where δ is the radius of the vortex core and L a typical longitudinal length. S is the length of the closed filament, and $C_v(t)$ and $C_w(t)$ are known functions that depend on the orthoradial and axial evolution of the inner velocity in the core. Equation (1) shows that the self-induced velocity of the filament

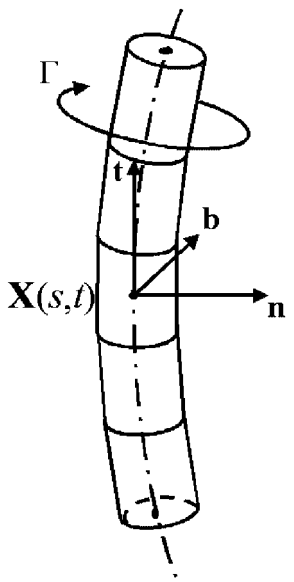

Figure 1. The filament centreline $\mathbf{X}(s,t)$ and the Frenet frame $(\mathbf{t},\mathbf{n},\mathbf{b})$.

is the sum of a local term in the binormal direction and a non-local one $\mathbf{A}(s,t)$ given by

$$\mathbf{A}(s,t)=\frac{\Gamma}{4\pi}\int_{-\pi}^{+\pi}\sigma(s+s',t)\left[\frac{\mathbf{t}(s+s',t)\times(\mathbf{X}(s,t)-\mathbf{X}(s+s',t))}{|\mathbf{X}(s,t)-\mathbf{X}(s+s',t)|^3}-\frac{K(s,t)\mathbf{b}(s,t)}{2|\lambda(s,s',t)|}\right]\mathrm{d}s'$$

where $\sigma(s,t)=|\partial\mathbf{X}/\partial s|$, and $\lambda(s,s',t)=\int_s^{s+s'}\sigma(s^*,t)\,\mathrm{d}s^*$.

2.2. *The core-structure functions $C_v(t)$ and $C_w(t)$*

The velocity field in the core is described by introducing the *local curvilinear co-ordinate system* $\mathbf{M}(r,\varphi,s)$ and the curvilinear vector basis $(\mathbf{e}_r,\mathbf{e}_\varphi,\mathbf{t})$. This system is defined in the following manner; if $\mathbf{P}(s)$ is the projection on the centreline $\mathbf{X}$ of a point $\mathbf{M}$ near the curve then $\mathbf{PM}$ is in the plane $(\mathbf{n},\mathbf{b})$ and thus polar co-ordinates (r,φ) can be used in this plane with the associated polar vectors $(\mathbf{e}_r,\mathbf{e}_\varphi)$. In the asymptotic theory [6] the relative velocity $\mathbf{V}$ is defined by $\mathbf{v}=\partial\mathbf{X}/\partial t+\mathbf{V}$ where $\mathbf{v}$ is the fluid velocity. We denote by (u,v,w) the radial, circumferential and axial components of $\mathbf{V}=u\mathbf{e}_r+v\mathbf{e}_\varphi+w\mathbf{t}$.

The expressions of the core-structure functions $C_v(t)$ and $C_w(t)$ are different depending on the initial leading-order velocity profiles in the core and on the viscosity of the fluid. In this subsection we successively give the velocity profiles and the core-structure functions $C_v(t)$ and $C_w(t)$ for an inviscid, similar and non-similar vortex core.

2.2.1. Inviscid vortex core. If the fluid is inviscid the leading-order circumferential and axial components of the relative velocity field are in the form [7]

$$v(\bar{r},t)=v_0(\bar{r}/\bar{\delta})[S_0/S(t)]^{-1/2}$$

$$w(\bar{r},t)=w_0(\bar{r}/\bar{\delta})S_0/S(t)$$

where $\bar{r} = r/\varepsilon$ is the stretched radial distance to the filament, $\bar{\delta} = \delta/\varepsilon$ is the stretched radius, $[v_0(\eta = \bar{r}/\bar{\delta}_0), w_0(\eta = \bar{r}/\bar{\delta}_0)]$ is the initial velocity field, and S_0 is the initial length of the filament. The ε-stretched radius $\bar{\delta}$ is

$$\bar{\delta}^2(t) = \bar{\delta}_0^2 S_0/S(t)$$

The inner functions are given by [7]

$$C_v(t) = C_v(0) - \log \bar{\delta}(t)$$

$$C_w(t) = C_w(0)[S_0/S(t)]^3$$

where $C_v(0)$ and $C_w(0)$ are the associated initial core constants.

2.2.2. Similar vortex core. The circumferential and axial components of the relative velocity field for a similar vortex are [7]

$$v(\bar{r}, t) = \frac{\Gamma}{2\pi\bar{r}}[1 - \mathrm{e}^{-(\bar{r}/\bar{\delta})^2}], \quad w(\bar{r}, t) = \frac{m_0}{\pi\bar{\delta}^2}\left(\frac{S_0}{S}\right)^2 \mathrm{e}^{-(\bar{r}/\bar{\delta})^2}$$

where $\bar{r}$ and $\bar{\delta}$ are defined as before, and m_0 is the initial axial flux of the vortex. The stretched radius $\bar{\delta}$ is given by [7]

$$\bar{\delta}^2(t) = \bar{\delta}_0^2 \left[\frac{S_0}{S(t)}\right] 1_{\bar{\nu}}$$

$$1_{\bar{\nu}} = 1 + \frac{\bar{\delta}_{\bar{\nu}}^2}{\bar{\delta}_0^2}$$

$$\bar{\delta}_{\bar{\nu}}^2 = 4\bar{\nu}\int_0^t \frac{S(t')}{S_0}\,\mathrm{d}t'$$

where $\bar{\nu} = \nu/\varepsilon^2$ is the stretched kinematic viscosity of the fluid of kinematic viscosity ν. The inner functions are given by [7]

$$C_v(t) = (1 + \gamma - \ln 2)/2 - \ln(\bar{\delta})$$

$$C_w(t) = -2(S_0/S)^4[m_0/(\Gamma\bar{\delta})]^2$$

where γ denotes Euler's constant. The effect of the diffusion is easily seen in these expressions through $\bar{\delta}_{\bar{\nu}}$ (the diffusion-added ε-stretched thickness of the core) in $\bar{\delta}$ and the influence of the stretching through the ratio S_0/S. The inviscid-similar vortex corresponds to $\bar{\nu} = 0$.

2.2.3. Non-similar vortex core. If the flow is viscous ($\bar{\nu} \neq 0$) and the core is non-similar, the circumferential and axial components of the relative velocity field are in

the form

$$v(\bar{r},t)=\frac{1}{\eta\bar{\delta}}\left[\frac{\Gamma}{2\pi}(1-\mathrm{e}^{-\eta^2})+\mathrm{e}^{-\eta^2}\sum_{n=1}^{\infty}\bar{\delta}_0^2 D_n P_n(\eta^2)1_{\bar{\nu}}^{-n}\right]$$

$$w(\bar{r},t)=\frac{2}{\bar{\delta}^2}\left[\frac{S_0}{S(t)}\right]^2\left[\frac{m_0}{2\pi}\mathrm{e}^{-\eta^2}+\mathrm{e}^{-\eta^2}\sum_{n=1}^{\infty}\bar{\delta}_0^2 C_n L_n(\eta^2)1_{\bar{\nu}}^{-n}\right]$$

where $\eta=\bar{r}/\bar{\delta}$ and the stretched radius $\bar{\delta}$ expression is the same as for a similar vortex. Here, L_n are the Laguerre polynomials, $P_n(\eta^2)=L_{n-1}(\eta^2)-L_n(\eta^2)$, and (C_n,D_n) are the Fourier components of the initial axial velocity w_0 and tangential vorticity $\zeta_0=[\partial(\bar{r}v_0)/\partial\bar{r}]/\bar{r}$:

$$C_n=\int_0^{\infty} w_0(\eta)L_n(\eta^2)\eta\,\mathrm{d}\eta$$

$$D_n=\int_0^{\infty}\zeta_0(\eta)L_n(\eta^2)\eta\,\mathrm{d}\eta$$

In particuliar we have $C_0=m_0/2\pi\bar{\delta}_0^2$, $D_0=\Gamma/2\pi\bar{\delta}_0^2$. The inner functions are given by

$$C_v(t)=-\log\bar{\delta}+\frac{1}{2}(1+\gamma-\log 2)+\frac{4\pi^2}{\Gamma^2}\sum_{(n,m)\in\mathbb{N}^2\setminus(0,0)}^{\infty}\frac{\bar{\delta}_0^4 D_n D_m A_{nm}}{n+m}1_{\bar{\nu}}^{-(n+m)}$$

$$C_w(t)=-\frac{2}{\bar{\delta}^2}\left[\frac{S_0}{S(t)}\right]^4\left[\frac{m_0^2}{\Gamma^2}+\frac{8\pi^2}{\Gamma^2}\sum_{(n,m)\in\mathbb{N}^2\setminus(0,0)}^{\infty}\bar{\delta}_0^4 C_n C_m A_{nm}1_{\bar{\nu}}^{-(n+m)}\right]$$

where

$$A_{nm}=\int_0^{\infty}\mathrm{e}^{-2x}L_n(x)L_m(x)\,\mathrm{d}x$$

$$=\frac{(n+m)!}{n!m!2^{m+n+1}}$$

Let us give two examples (Figure 2) of non-similar cores with the same circulation as the similar vortex $\zeta_0(\eta)=\Gamma\exp(-\eta^2)/\pi\bar{\delta}_0^2$ of thickness $\bar{\delta}_0$. The first one is the Rankine vortex:

$$\zeta_0(\eta)=\begin{cases}\dfrac{\Gamma}{\pi\bar{\delta}_0^2} & \text{if } \eta<1\\[2ex] 0 & \text{if } \eta>1\end{cases}$$

The second one is the *witch-hat* vortex:

$$\zeta_0(\eta)=\begin{cases}\dfrac{\Gamma}{\pi\bar{\delta}_0^2}\left(1-\dfrac{\eta}{\sqrt{3}}\right) & \text{if } \eta<\sqrt{3}\\[2ex] 0 & \text{if } \eta>\sqrt{3}\end{cases}$$

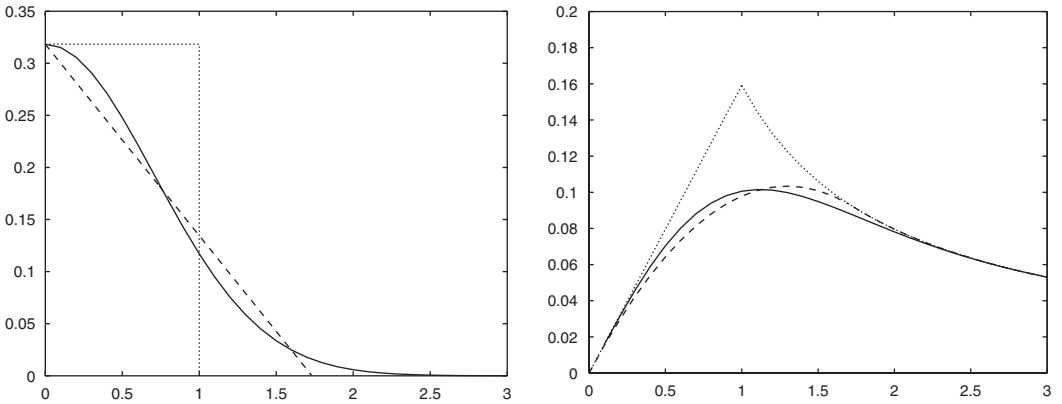

Figure 2. Vorticity $\zeta_0\bar{\delta}_0^2/\Gamma$ (left) and circumferential velocity $v_0\bar{\delta}_0/\Gamma$ (right) versus $\eta = \bar{r}/\bar{\delta}_0$. The solid line is for the similar vortex, the dotted line for the Rankine vortex and the dashed line for the witch-hat vortex.

2.3. *The Local Induction Approximation (LIA) equation*

The local induction approximation (LIA) equation is

$$\partial\mathbf{X}/\partial t = \frac{\Gamma K(s,t)}{4\pi}\left[-\log\varepsilon + \log(S) - 1 + C_v(t) + C_w(t)\right]\mathbf{b}(s,t) \tag{2}$$

In this approximation the non-local self-induction $\mathbf{A}(s,t)$ of Equation (1) is not taken into account. This regular term is indeed negligible in the small ε limit.

2.4. *A simple de-singularized method for a closed filament*

One of the simplest justified de-singularized equation is [9]

$$\partial\mathbf{X}/\partial t = \frac{\Gamma}{4\pi}\int_{-\pi}^{\pi}\sigma(s',t)\,\frac{\mathbf{t}(s',t)\times[\mathbf{X}(s,t)-\mathbf{X}(s',t)]}{[|\mathbf{X}(s,t)-\mathbf{X}(s',t)|^2 + s_c^2]^{3/2}}\,\mathrm{d}s' \tag{3}$$

with

$$s_c(s,t) = \varepsilon\exp[-C_v(t) - C_w(t)] \tag{4}$$

This method is very easy to implement. However, as already explained in the introduction, this equation is still stiff to be solved numerically and so needs extra discretized elements near the point on the curve where the velocity is to be computed.

2.5. *The M1 de-singularized method of Knio and Klein for a closed filament*

The M1 de-singularized equation of Knio and Klein [17, 18] is

$$\partial\mathbf{X}/\partial t = \mathbf{v}_{\sigma_1} + (\mathbf{v}_{\sigma_1} - \mathbf{v}_{\sigma_2})\,\frac{\log(\sigma_1/\delta^{ttm})}{\log(\sigma_2/\sigma_1)} \tag{5}$$

where

$$\mathbf{v}_{\sigma_i} = \frac{\Gamma}{4\pi} \int_{-\pi}^{\pi} \sigma(s',t) \frac{\mathbf{t}(s',t) \times [\mathbf{X}(s,t) - \mathbf{X}(s',t)]}{|\mathbf{X}(s,t) - \mathbf{X}(s',t)|^3} \kappa \left(\frac{|\mathbf{X}(s,t) - \mathbf{X}(s',t)|}{\sigma_i} \right) \mathrm{d}s', \quad i = 1,2 \tag{6}$$

with $\kappa(r) = \tanh(r^3)$ and

$$\delta^{ttm} = \varepsilon \exp(C^{ttm} + 1 - C_v(t) - C_w(t)) \tag{7}$$

$$\sigma_1 = 3\sigma_{\max} \tag{8}$$

$$\sigma_2 = 2\sigma_1 \tag{9}$$

$$\sigma_{\max} = \mathrm{d}s \max_{s \in [0,2\pi]} \sigma(s,t) \tag{10}$$

With the choice of $\kappa(r) = \tanh(r^3)$, the C^{ttm} constant is $C^{ttm} = -0.4202$ as obtained by Knio and Klein [18]. It can be computed from Equations (4.23), (4.22) and (3.23) of Klein and Knio [17] with a change of sign of $\zeta_{11}^{(1),ttm}$ in their Equation (4.23).

Through a direct matched asymptotic expansion in σ_i of (6) and a comparison of the associated expanded equation of motion with the Callegari and Ting (1) equation of motion we obtain the following expression of the C^{ttm} constant:

$$C^{ttm} = -\log(4) + \int_0^2 \kappa(s)/s \, \mathrm{d}s + \int_2^{\infty} \frac{\kappa(s) - 1}{s} \mathrm{d}s$$

for any function $\kappa(s)$ such that $\kappa(s) = 1$ at infinity. The choice of $\kappa(r) = 4\pi \int_0^r \xi^2 f(\xi) \, \mathrm{d}\xi$ with $f(r) = \pi^{-3/2} \exp(-r^2)$ can be analytically computed and gives $C^{ttm} = -1 + 0.5\gamma$ where γ is the Euler's constant.

2.6. *Mutual induction and open filaments*

In case of several filaments $\mathbf{X}_j$ their induced velocities

$$\frac{\Gamma_j}{4\pi} \int_{\mathscr{C}_j} \sigma_j(s',t) \frac{\mathbf{t}_j(s',t) \times (\mathbf{X}(s,t) - \mathbf{X}_j(s',t))}{|\mathbf{X}(s,t) - \mathbf{X}_j(s',t)|^3} \mathrm{d}s' \tag{11}$$

are added to the self-induced velocity of $\mathbf{X}$.

A periodic open filament of wavelength $\Lambda(t)$ in the axial $\mathbf{e}_x$ direction satisfies $\mathbf{X}(s + 2\pi, t) = \mathbf{X}(s,t) + \Lambda(t)\mathbf{e}_x$. From Callegari and Ting's equation [6] one can deduce the following equation for such a filament:

$$\partial \mathbf{X}/\partial t = \Gamma K(s,t)[-\ln \varepsilon + \ln \Lambda(t) - 1 + C_v(t) + C_w(t)]\mathbf{b}(s,t)/4\pi + \mathbf{A}(s,t) \tag{12}$$

where $\mathbf{A}(s,t)$ is the non-local self-induction of the filament and is given by

$$\mathbf{A}(s,t) \equiv \frac{\Gamma}{4\pi} \int_{-\infty}^{+\infty} \sigma(s+s',t) \left[\frac{\mathbf{t}(s+s',t) \times [\mathbf{X}(s,t) - \mathbf{X}(s+s',t)]}{|\mathbf{X}(s,t) - \mathbf{X}(s+s',t)|^3} \right.$$

$$\left. - H\left(\frac{\Lambda(t)}{2} - |\lambda(s,s',t)| \right) \frac{K(s,t)\mathbf{b}(s,t)}{2|\lambda(s,s',t)|} \right] \mathrm{d}s'$$

where H is the Heaviside function. The expression of the core-structure functions can be obtained by replacing the finite length $S(t)$ by the wavelength $\Lambda(t)$ of the periodic filament in the previous expressions of a closed vortex. In the same way as Equation (1) for closed filaments becomes Equation (12) for periodic open filaments, one can easily find the equations for periodic open filaments associated to Equations (2), (3) and (5).

2.7. Axial flow velocity and viscosity

Equations (1), (3) and (5) are indeed different formulations of the same equation. They will lead to different numerical discretizations with more or less advantages.

All of these equations handle cases where the axial flow is non-zero ($C_w \neq 0$) and the viscosity is non-zero ($\bar{\nu} \neq 0$). Viscosity appears in terms $\bar{\delta}$ and $1_{\bar{\nu}}$ in the core functions C_v and C_w (Section 2.2.3), where the thickness $\bar{\delta}$ and the coefficient $1_{\bar{\nu}}$ are given in Section 2.2.2.

This general case is implemented in our code even if we will only present simulations with non-axial flow velocity and no viscosity in Sections 4 and 5. The reader can find numerical simulations with axial flow and viscosity in Reference [8] for closed filaments.

3. NUMERICAL DISCRETIZATION AND IMPLEMENTATION

The code EZ-vortex [19] is the numerical implementation of Equations (1), (2), (3), and (5) for closed filaments and of the associated versions for open filaments including Equation (12). The philosophy of the code is to keep programs as simple as possible and to provide documentation both by way of a text [19] and comments within the code itself. It is available through the world-wide web and is adapted from the code EZ-Scroll developed by Dwight Barkley for simulating scroll waves in excitable media [20, 21]. This package uses OpenGL for 3D rendering or the Mesa library (public domain implementation of most OpenGL routines). It should be possible to run on virtually any machine supporting X. Setting macros of the C-preprocessor (defined in the main header file) to 0 or 1 allows to have a conditional compilation of the code and to have a unique source-code with different equations of motion and with different spatial and temporal numerical discretizations.

The *physical* parameters in the simulation are the initial stretched core radius $\bar{\delta}_0$, the initial axial flux m_0, the circulation Γ, the aspect ratio parameter $\varepsilon = \delta/L$, and the stretched viscosity $\bar{\nu} = \nu/\varepsilon^2$ of the fluid. The *numerical* parameters for the simulation are the number np of spatial points (nodes) on each filament, the time step dt, the number nsteps of time steps and nb the number of periodic boxes for open filaments (see Figure 3). The integral in the formulation of $\mathbf{A}(s,t)$ (Equation (12)) is evaluated over $s' \in]-\mathsf{nb}\Lambda, +\mathsf{nb}\Lambda[$ instead of $s' \in]-\infty, +\infty[$. The missing part of the integral quickly decreases when the number of boxes nb increases. In our computer code open filaments can be therefore considered as infinitely long periodic filaments of wavelength Λ.

3.1. Spatial discretization

The curve $\mathbf{X}$ is discretized by putting np points on the centreline, i.e. by an uniform discretization of the interval $s \in [-\pi, \pi[$.

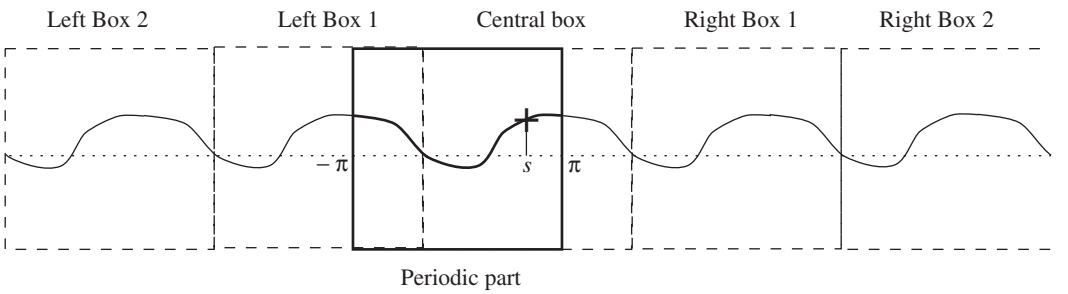

Figure 3. Periodic part of the filament, central box around $\mathbf{X}(s,t)$ and left and right side boxes.

3.1.1. Derivatives. First-derivative $\sigma\mathbf{t} = \partial\mathbf{X}/\partial s$ and second-derivative $K\mathbf{b} = \partial\mathbf{X}/\partial s \times \partial^2\mathbf{X}/\partial s^2 / |\partial\mathbf{X}/\partial s|^3$ are approximated by second order centred differences or spectrally computed via a fast Fourier transform (FFT). For periodic open filament in the $\mathbf{e}_x$ direction $[\mathbf{X}(s+2\pi,t) = \mathbf{X}(s,t) + \Lambda(t)\mathbf{e}_x]$ the following periodic function $\tilde{\mathbf{X}}(s,t) = \mathbf{X}(s,t) - \Lambda(t)s/(2\pi)\mathbf{e}_x$ is defined. As it satisfies $\tilde{\mathbf{X}}(s+2\pi,t) = \tilde{\mathbf{X}}(s,t)$ its derivatives can be spectrally computed via a FFT as for the closed filament. The first-derivative is then given by $\partial\mathbf{X}/\partial s = \partial\tilde{\mathbf{X}}/\partial s + \Lambda(t)/(2\pi)\mathbf{e}_x$ and the second-derivative by $\partial^2\mathbf{X}/\partial s^2 = \partial^2\tilde{\mathbf{X}}/\partial s^2$.

3.1.2. Integrals. The trapezoidal rule is used to compute any integral part of the equation of motion. In case of a periodic open filament we take advantage of the periodicity and advance in time only a part of the filament (see Figure 3) corresponding to a period $\Lambda(t)$ (or an integer number of periods). The self-induction at point $\mathbf{X}(s,t)$ on this part of the filament is found by adding two contributions (see Figure 3). The first one is the self-induction of a bit of filament in a box of length $\Lambda(t)$ centred on $\mathbf{X}(s,t)$. The second is the induction of the remaining part of the open filament in nb boxes of length $\Lambda(t)$ from both sides of the central box. The self-induction part is obtained with one of Equations (1), (2), (3) or (5) for a closed filament and the remaining part is obtained with the mutual induction velocity formula (11) as if it were coming from other filaments.

The spatial discretization can be checked at initial time by testing the convergence of the Biot–Savart velocity computation with the number of points and with the number of periodic boxes for open filaments.

3.2. Temporal discretization

The time stepping of the equation of motion is either an explicit forward Euler first-order scheme, an implicit backward Euler first-order scheme with an iterative sequel that converges to the solution of the non-linear algebraic system, or an Adams–Bashforth second-order explicit scheme. Explicit schemes can also be done *on place*, i.e. without a temporary variable for the co-ordinate positions for the nodes of the filament.

Explicit schemes for equations with a local $K\mathbf{b}$ term [Callegari and Ting (1) or LIA (2)] are always unstable [22] and are conditionally stable for the simple de-singularized method (3) or for the M1 de-singularized method (5) of Knio and Klein. An Adams–Bashforth second-order explicit scheme can be used with these later methods. Moreover (3) and (5) need not to compute the local $K\mathbf{b}$ term and are also easier to implement because their non-local integral

term is a simple expression whereas in the Callegari and Ting Equation (1) the integrand of the integral term **A** is a subtraction of two terms and needs the computation of the $K\mathbf{b}$ term and of the integral distance function $\lambda(s,s',t)$. The M1 de-singularized method of Knio and Klein (5) is more advantageous than the simple de-singularized method (3) because contrary to this later method it is not stiff in the small thickness parameter ε: as can be seen from direct numerical computation the simple de-singularized method (3) needs much more number of points to converge than the M1 de-singularized method of Knio and Klein. It is interesting to have implemented all these different methods in order to compare their different advantages from direct numerical computation and to avoid any implementing mistake by checking their convergence to the same result. The convergence of every simulation is assessed by increasing the number of points and by decreasing the time step.

3.3. *Closed and open filament storage*

In this subsection we explain the choices we did to implement the numerical schemes. It is of interest for anyone who would like to do such an implementation or go through the lines of the EZ-vortex code. Cartesian co-ordinates (x,y,z) of nodes i on the filament j are successively stored in a pointer u and are managed by three macros Ux(i,j), Uy(i,j), Uz(i,j), where Ux(i,j) is the co-ordinate x of the node i on the filament j. The same kind of pointer (u_s, u_ss, ...) and macros are used for the first and second derivatives, for σ and for the velocity components. The index i ranges from 0 to np + 1 and the index j from 0 to nf − 1, where np and nf are respectively the number of nodes and of filaments. Points 0 and np + 1 are added-fictitious points which may be of use.

For a closed filament the point of index np is at the same location as the point of index 1, whereas for an open filament the point of index np is the translated point [with period $\Lambda(t)$] of the point of index 1. In the spectral computation of the derivatives the FFT routine uses the points from $i=1$ to $i=$ np − 1 and the index np − 1 is 256. For closed filaments we find the induced velocity on nodes $i=1$ to $i=$ np − 1 (respectively, $i=$ np for open filament) and then move all these points.

For open filaments the self-induced velocity at any point $\mathbf{X}(s,t)$ of index i is found as displayed in Figure 3: temporary pointers (ux_tmp, uy_tmp, uz_tmp) are introduced to store part of the filament in the *central box* around this point i which is stored at the central index (np+1)/2 of these pointers (the number of points np is an odd number). The same temporary pointers are also used for closed filaments. With these temporary pointers the same procedure is then used to compute the velocity whatever point is under consideration. The procedure to fill these pointers is different whether the filament is closed or open because indices have to be managed differently. For open filaments the induced velocity of the nb copies on the left and right boxes is added to the self-induced velocity of the central part.

4. VALIDATION AGAINST EXACT SOLUTIONS AND LINEAR STABILITY RESULTS

In this section we validate the code EZ-vortex against known solutions of the equations of motion for the centreline and results of linear stability studies. We also give the values of the numerical parameters that give converged numerical results for the different configurations

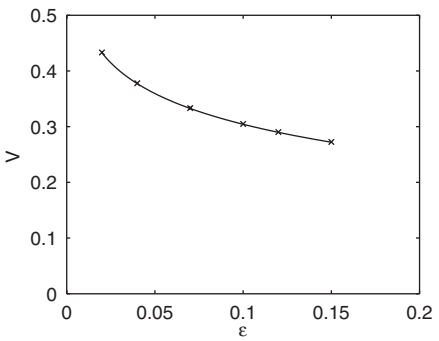

Figure 4. Velocity V of the vortex ring versus ε. The solid line is from the analytical result and crosses from numerical computation (Run 1 in Table I).

Table I. Numerical parameters: closed vortices.

	Run	*np*	*dt*	*nsteps*	CPU time*(s)
Circular vortex ring (M1)	1	101	0.0016	7000	79.8
Circular vortex ring (CT)	2	101	0.0016	7000	186
Perturbed vortex ring	3	257	0.0016	250	17
Vortex ring pair	4	101	0.00008125	7000	1200

* SGI R10000 work-station at 225 MHz.

under consideration. All following simulations use the M1 de-singularized method of Knio and Klein with the explicit Adams–Bashforth scheme, there is no axial flow ($m_0 = 0$) and the fluid is inviscid ($\bar{\nu} = 0$). Here, the vortex core is similar and $\Gamma = 1$. As the initial reduced thickness is $\bar{\delta}_0 = 1$ the small parameter ε is the initial thickness δ_0.

4.1. The perturbed circular vortex ring

The velocity of a circular vortex ring of radius R and thickness δ is [23]

$$V = \frac{\Gamma}{4\pi R}\left(\log\frac{8R}{\delta} + C_v - 1 + C_w\right) \tag{13}$$

For a similar core without axial velocity $C_v = 0.442$ and $C_w = 0$. In Figure 4 we plot the velocity V of the vortex ring of radius $R = 1$ as a function of the initial thickness ε. Numerical results (crosses) are in excellent agreement with the analytical result (solid line). The numerical parameters of the computation are given in Table I for the M1 method of Knio and Klein with the explicit Adams–Bashforth scheme (Run 1) or for the Callegari and Ting equation with an implicit iteration (Run 2).

The period T of a modal perturbation with azimuthal wave number n is

$$T = \frac{8\pi^2 R^2}{\Gamma\sqrt{[n^2\tilde{V}_0 - g_\xi(n)][(n^2-1)\tilde{V}_0 + g_\rho(n)]}} \tag{14}$$

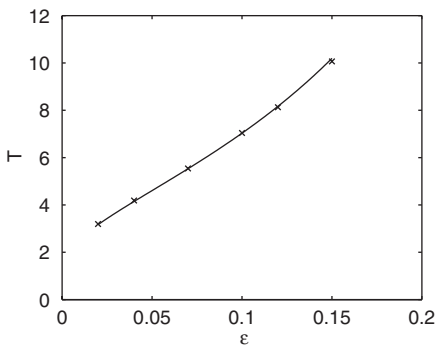

Figure 5. Period T for the mode 3 of the perturbed vortex ring versus ε. Same legend as in Figure 4.

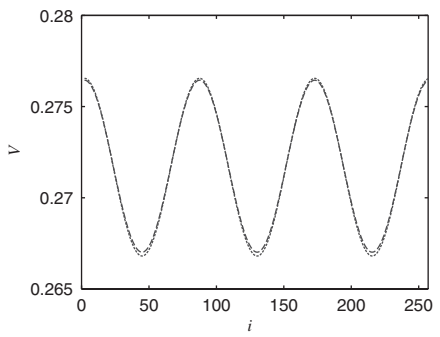

Figure 6. Binormal velocity V at initial time for the mode 3 of the perturbed vortex ring $\varepsilon = 0.15$ versus the node number i of the filament. The solid line is the M1 Knio and Klein method and the dashed line is the Callegari and Ting equation. Same parameters as in Figure 5.

where $\tilde{V}_0 = 4\pi RV/\Gamma$ and $[g_\xi(n), g_\rho(n)]$ are given in Margerit *et al.* [23]. In Figure 5 we plot the period T for the mode 3 of the perturbed vortex ring as a function of ε. Numerical results (crosses in Figure 5 and Run 3 in Table I) are in excellent agreement with the analytical result (solid line). The initial amplitude of the perturbation is $\rho_0 = 0.01$ with the centreline in a plane. This period is found by using $\rho_\perp$ the amplitude part orthogonal to the propagating direction x. It is given by $\rho_\perp = \text{abs}[\sqrt{Z^2 + Y^2} - \text{mean}(\sqrt{Z^2 + Y^2})]$ where $\mathbf{X} = (X, Y, Z)$ and where *mean* is the spatial average on the filament at time t. The pulsation is then found with the slope of the temporal function $\arccos[\rho_\perp/\rho_\perp(0)]$. This slope does not depend on the point of abscisse s that is used. In practice we do not choose any point and use the maximum of $\rho_\perp$ over the filament. It converges with all numerical parameters (time step, number of points) and with decreasing initial amplitude ρ_0.

The period at $\varepsilon = 0.15$ is not exactly on the curve. This small difference comes from finite ε effect. M1 Knio and Klein method and Callegari and Ting equation has been proved to be equivalent in the asymptotic small ε limit. When $\varepsilon = 0.15$ we notice (Figure 6) a difference of the Biot–Savart results given by these two methods whereas there is no difference for $\varepsilon = 0.02$. We believe that this difference is due to the next-order correction in ε which may no longer

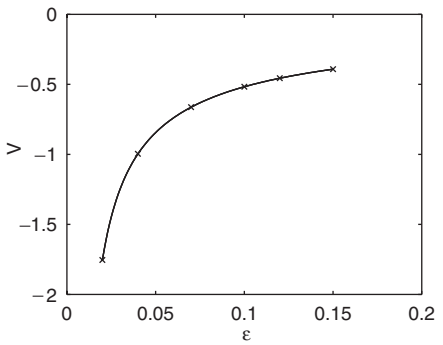

Figure 7. Velocity V of the vortex ring pair versus ε for $R = 0.5$. Same legend as in Figure 4.

be neglected at $\varepsilon = 0.15$. All methods and stability equations are equivalent at leading order but may be slightly different due to the effect of next-order correction.

4.2. Motion of a vortex ring pair

We consider two circular vortex rings in the same plane with same centre and thickness δ. Let Γ_o, Γ_i, R_o and R_i denote the circulations and the radius of the outer and inner vortices. We introduce the dimensionless parameters $R = R_i/R_o$ and $G = \Gamma_i/\Gamma_o$. There is an exact stationary solution of the equation of motion (1) provided that the following relation between G and R is satisfied [24]

$$G = \frac{E(k)/(1-R) + K(k)/(1+R) - 0.5[\log(8R_0/\delta) + C_v - 1 + C_w]}{-E(k)/(1-R) + K(k)/(1+R) - 0.5[\log(8R_i/\delta) + C_v - 1 + C_w]/R} \tag{15}$$

where $k = 2\sqrt{R}/(1+R)$. Here E and K are complete elliptic integrals of second and first kinds. The associated velocity V is

$$V = \frac{\Gamma_i}{4\pi R_i}[\log(8R_i/\delta) + C_v - 1 + C_w] + \frac{\Gamma_o}{2\pi R_o}[E(k)/(1-R) + K(k)/(1+R)] \tag{16}$$

In Figure 7 we plot the velocity V of the vortex ring pair as a function of ε for $R = 0.5$ and $\Gamma_i = 1$. Numerical results (crosses in Figure 7 and Run 4 in Table I) are in excellent agreement with the analytical result (solid line).

4.3. The perturbed straight filament

The period of rotation of a sinusoidal perturbation on a straight filament is

$$T = \frac{8\pi^2}{\Gamma k^2 |1/2 - \gamma + \log(2/\delta k) + C_v - 1 + C_w|} \tag{17}$$

where $\gamma = 0.577215$, δ is the core radius, Γ is the circulation and $k = 2\pi/\Lambda$ is the wave number. This result generalizes to an arbitrary vorticity profile the classical Kelvin [25] result for the bending modes of a Rankine vortex for small wave numbers. Kelvin obtained it by

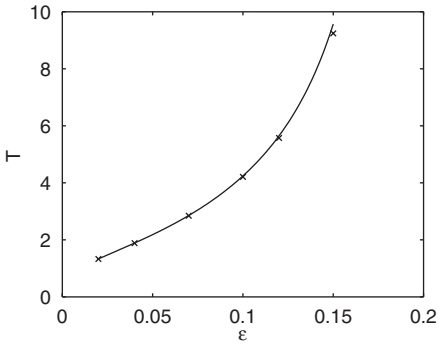

Figure 8. Period T for the wavelength $\Lambda = 1.25$ of the perturbed straight vortex filament versus the initial thickness ε. Same legend as in Figure 4.

Table II. Numerical parameters: open vortices.

	Run	Λ	*np*	*dt*	*nb*	*nsteps*	CPU time*(s)
Straight filament	5	1.25	257	0.00026	8	600	330
Oscillations of a vortex pair	6	1.25	257	0.00026	8	250	516
Instability of a vortex pair	7	10.21	101	0.0019	8	800	240
Instability of a vortex pair (non linear (NL) regime)	8	10.21	101	0.0019	8	7950	2520
Four vortices (most amplified S1 mode)	9	0.8976	61	0.0019	20	250	264
Four vortices (most amplified S1 mode NL regime)	10	0.8976	61	0.0019	20	872	930
Four vortices (long-wave S1 or A mode)	11	7.85	101	0.0019	8	250	306
Four vortices (long-wave S1 or A mode NL regime)	12	7.85	101	0.0019	8	1744	2160

* SGI R10000 work-station at 225 MHz.

considering infinitesimal perturbations to a columnar vortex; we obtained it by infinitesimal perturbations to the straight centreline in (12).

In Figure 8 we plot the period T for the wavelength $\Lambda = 1.25$ of the perturbed straight vortex filament as a function of ε. Numerical results (crosses in Figure 8 and Run 5 in Table II) are in excellent agreement with the analytical result (solid line). The initial amplitude of the perturbation is $\rho_0 = 0.01$. This period is found by using ρ_y the amplitude part in the y direction. It is given by $\rho_y = \text{abs}(Y - \bar{Y})$ where $\mathbf{X} = (X, Y, Z)$ and where $\bar{Y}$ is the spatial average on the filament at time t. The pulsation is then found with the slope of the temporal function $\arccos[\rho_y/\rho_y(0)]$.

5. STUDY OF A TWO-VORTEX AIRCRAFT WAKE

In this section the EZ-vortex code is used to study a two-vortex aircraft wake which consists in a pair of contra-rotating vortex filaments. It also gives another validation of the code. As in the previous section all following simulations use the M1 de-singularized method of Knio and Klein with the explicit Adams–Bashforth scheme and with $\Gamma = \pm 1$. There is no axial flow

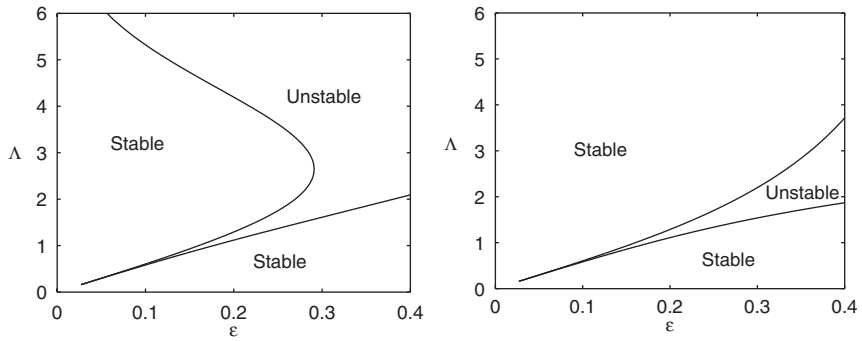

Figure 9. Stability diagram for symmetric (left) and antisymmetric (right) modes of a similar vortex pair without axial flow: Λ is the wavelength and ε is the initial thickness.

($m_0 = 0$) and the fluid is inviscid ($\bar{\nu} = 0$). Here, the vortex core is a *similar vortex* profile. The initial reduced thickness is $\bar{\delta}_0 = 1$ and so the small parameter ε is the initial thickness δ_0. The velocity of the contra-rotating vortex filament pair of circulation $\pm\Gamma$ is $V = \Gamma/2\pi b$, where b is the distance between the vortices. We checked that the code reproduces this velocity (data not shown). The stability diagrams can be deduced from the study of Crow [10] and are recalled in Figure 9. Here, we chose to display the wavelength instead of the wave number and to plot the diagrams as a function of the initial thickness ε rather than the *ad hoc* cut-off length of Crow [10]. These diagrams are in dimensionless form ($b = 1$ and $\Gamma = \pm 1$).

The period of the symmetric stable modes is [10]

$$T = \frac{4\pi^2 b^2}{\Gamma\sqrt{-(1 - \psi + k^2 b^2 \tilde{\omega})(1 + \chi - k^2 b^2 \tilde{\omega})}} \tag{18}$$

where $k = 2\pi/\Lambda$ is the wave number and

$$\psi = k^2 b^2 K_0(kb) + kbK_1(kb)$$
$$\chi = kbK_1(kb)$$
$$\tilde{\omega} = \left(-1 + \log\frac{2}{\delta k} + 1/2 - \gamma + C_v + C_w\right)/2$$

Here, K_0 and K_1 are modified Bessel functions of the second kind. The period of the anti-symmetric modes is given by [10]

$$T = \frac{4\pi^2 b^2}{\Gamma\sqrt{-(1 + \psi + k^2 b^2 \tilde{\omega})(1 - \chi - k^2 b^2 \tilde{\omega})}} \tag{19}$$

Figure 10 shows the period T for the wavelength $\Lambda = 1.25$ of the perturbed contra-rotating filaments (symmetric stable modes) as a function of the initial thickness ε. Numerical results (crosses in Figure 10 and Run 6 in Table II) are in excellent agreement with the analytical result (solid line). This period is found in the same way as in Section 4.3.

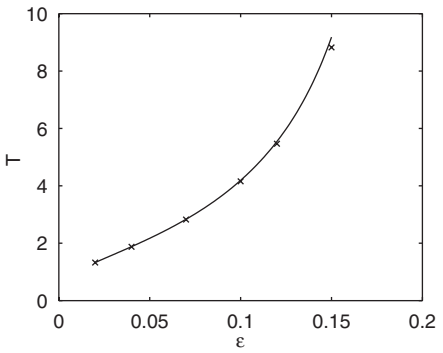

Figure 10. Period T for the wavelength $\Lambda = 1.25$ of the perturbed contra-rotating vortex pair (symmetric stable modes) versus its initial thickness ε. Same legend as in Figure 4.

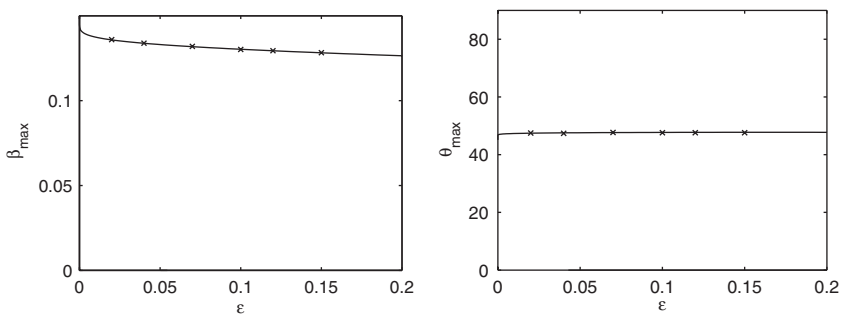

Figure 11. Growth rate $\beta_{\max}$ (left) and planar angle $\theta_{\max}$ (right) versus the initial thickness ε for the most unstable wavelength of the perturbed contra-rotating vortex pair (symmetric unstable mode). Same legend as in Figure 4.

The growth rate β of the symmetric unstable modes is [10]

$$\beta = \frac{1}{8\pi b^2}\sqrt{(1-\psi+k^2b^2\tilde{\omega})(1+\chi-k^2b^2\tilde{\omega})} \tag{20}$$

The growing perturbations are planar standing waves with planes fixed at angle θ to the horizontal [10]:

$$\theta = \arctan\left(\sqrt{(1+\chi-k^2b^2\tilde{\omega})/(1-\psi+k^2b^2\tilde{\omega})}\right) \tag{21}$$

Figure 11 displays the growth rate $\beta_{\max}$ and the planar angle $\theta_{\max}$ for the most unstable wavelength $\Lambda(\varepsilon)$ (symmetric unstable mode) of the perturbed contra-rotating vortex pair as a function of the initial thickness ε. Numerical results (crosses in Figure 11 and Run 7 in Table II) are in excellent agreement with the analytical results (solid line). The initial amplitude of the perturbation is $\rho_0 = 0.001$ and the initial planar angle is deduced from (21). It has been checked that the planar angle of the mode did not change during the computation:

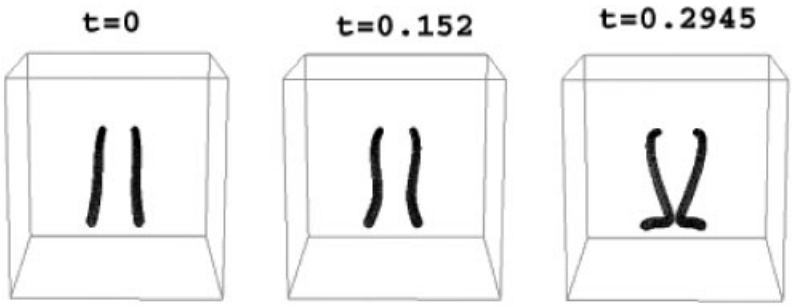

Figure 12. Vortex filament simulation of the non-linear instability regime of the most unstable mode $\Lambda = 10.21$ for the contra-rotating vortex pair. Initial amplitude $\rho = 0.05$, initial thickness $\varepsilon = 0.02$ and initial angle $\theta(t=0) = 47.63(\text{deg})$.

reported crosses are the value of this angle at the end of the computation. The amplitude $\rho(s,t)$ is given by $\rho^2(s,t) = [Z(s,t) - \bar{Z}(t)]^2 + [Y(s,t) - 0.5]^2$ where $\mathbf{X} = (X, Y, Z)$ and where $\bar{Z}(t)$ is the spatial average on the filament at time t. The growth rate is given by the slope of the temporal function $\log[\rho(s,t)/\rho(0)]$. It converges with all numerical parameters (time step, number of points and number of boxes) and with decreasing initial amplitude ρ_0. With an axial flux ($m_0/\Gamma \neq 0$) the ε axis of the previous figures is multiplied by $\exp(-2[m_0/\Gamma]^2)$. We checked that analytical and numerical results also agree for $m_0/\Gamma = 0.6$.

Figure 12 displays the evolution of the Crow instability of the most unstable mode in the non-linear regime (Run 8 in Table II). For sake of clarity the curve of the centreline is represented by a tube with an arbitrary core radius.

Viscous and non-similar effects are implemented in EZ-vortex but could not be validated by lack of known analytical results. The linear growth rate β found from the first time steps as before is almost constant with the viscous parameter $\bar{\nu} = \nu/\varepsilon^2$ till $\simeq 4$. The maximum amplitude on the filament $\rho(t)$ as a function of time is weakly affected by the viscosity ($\bar{\nu} = 1$) in the non-linear regime. The simulations of the Rankine or the *witch-hat* profiles give almost the same maximum amplitude $\rho(t)$ evolution as for a similar core.

6. STUDY OF A FOUR-VORTEX AIRCRAFT WAKE

In this section the EZ-vortex code is used to study a four-vortex aircraft wake. It also gives a last validation of the code. As in the previous sections all following simulations use the M1 de-singularized method of Knio and Klein with the explicit Adams–Bashforth scheme, there is no axial flow ($m_0 = 0$) and the fluid is inviscid ($\bar{\nu} = 0$). Here, the vortex core is a *Rankine* profile. The two trailing vortex pairs have the same axis of symmetry. Let us denote Γ_o, Γ_i, b_o, b_i, $\bar{\delta}_o(t=0)$ and $\bar{\delta}_i(t=0)$ the circulations, the distances and the thickness of the outer and inner vortex pairs. We introduce the dimensionless parameters $R = b_i/b_o$ and $G = \Gamma_i/\Gamma_o$. The initial outer reduced thickness is $\bar{\delta}_o(t=0) = 1$ and so the small parameter ε is the initial thickness of the outer pair.

Table III. Four-vortex modes: linear stability (th.) and EZ-vortex (num.) results at $\varepsilon = 0.1$.

	Λ	β	θ_o(deg)	θ_i(deg)	$\varrho = \rho_i/\rho_o$
Most amplified S1 mode (th.) [27]*	0.8976	2.91	105.86	131.24	57.4
Most amplified S1 mode (num. Run 9 in Table II)	0.8976	2.94	111.04	130.20	52.8
Long-wave S1 mode (th.) [27]*	7.85	1.55	145.45	103.85	9.72
Long-wave S1 mode (num. Run 11 in Table II)	7.85	1.56	145.68	103.73	9.80
Long-wave A mode (th.) [27]*	7.85	1.469	116.90	167.03	9.58
Long-wave A mode (num. Run 11 in Table II)	7.85	1.511	118.72	166.39	9.73

*Results given by D. Fabre.

There is an exact stationary solution of the equation of motion (12) provided that the following relation between G and R is satisfied [26]

$$G = -\frac{3R + R^3}{3R^2 + 1} \tag{22}$$

The associated velocity V is

$$V = \frac{\Gamma_i}{2\pi b_i} + \frac{2\Gamma_o}{\pi b_o}\frac{1}{1 - R^2} \tag{23}$$

We checked that the EZ-vortex code reproduces this velocity for the ratio $R = 0.14$ (associated G is -0.4.) used by Fabre and Jacquin [27].

As for the contra-rotating vortex pair sinusoidal unstable modes exist. The growing perturbations are planar with planes fixed at angles θ_o (outer trailing pair) and θ_i (inner trailing pair) with respect to the horizontal [27]. Let $\varrho = \rho_i/\rho_o$ be the ratio of the amplitudes. Fabre and Jacquin [27] carried out the linear stability study of this wake and gave results for $R = 0.14$ ($G = -0.4$), $\varepsilon = 0.1$, $\bar{\delta}_o(t = 0) = 1$, $\bar{\delta}_i(t = 0) = 0.5$, $\Gamma_o = 1$ and $b_o = 1$. The growth rates and the associated modes of the most amplified S1 mode $\Lambda = 0.8976$ and for the long-wave S1 and A modes $\Lambda = 7.85$ are given in Table III. We have reproduced these results with the EZ-vortex code by starting from a perturbation amplitude $\rho_0 = 0.001$. The growth rate β is obtained from the slopes of the temporal functions $\log[\rho_\alpha(s,t)/\rho_\alpha(0)]$ with the amplitudes $\rho_o(s,t)$ and $\rho_i(s,t)$ measured by

$$\begin{aligned} \rho_o^2(s,t) &= [Z_o(s,t) - \bar{Z}_o(t)]^2 + [Y_o(s,t) - \bar{Y}_o(t)]^2 \\ \rho_i^2(s,t) &= [Z_i(s,t) - \bar{Z}_i(t)]^2 + [Y_i(s,t) - \bar{Y}_i(t)]^2 \end{aligned} \tag{24}$$

where $\mathbf{X}_\alpha = (X_\alpha, Y_\alpha, Z_\alpha)$ and $\bar{Z}_\alpha(t)$ and $\bar{Y}_\alpha(t)$ are the spatial averages on the filament $\alpha = o$ or i at time t. We start with the linear stability results and carry out several computations starting with $\rho_0 = 0.001$ and with $(\theta_o, \theta_i, \varrho = \rho_i/\rho_o)$ from the final values of previous computation. It converges to fixed values reported in Table III. We have carried out the same comparison for $\varepsilon = 0.02$ and shown that the small difference between numerical and linear stability results disappears (Table IV). This difference is thus due to finite ε effects. Figure 13 displays the evolution of these modes in the non-linear regime. The numerical parameters of the computation are given in Table II (Runs 10 and 12).

Table IV. Four-vortex modes: linear stability (th.) at $\varepsilon = 0.02$.

	Λ	β	θ_o(deg)	θ_i(deg)	$\varrho = \rho_i/\rho_o$
Most amplified S1 mode (th.)*	1.2566	3.07	82.81	132.53	48.5
Long-wave S1 mode (th.)*	7.85	1.62	140.36	104.35	10.00
Long-wave A mode (th.)*	7.85	1.40	110.13	167.54	9.35

* Results given by D. Fabre.

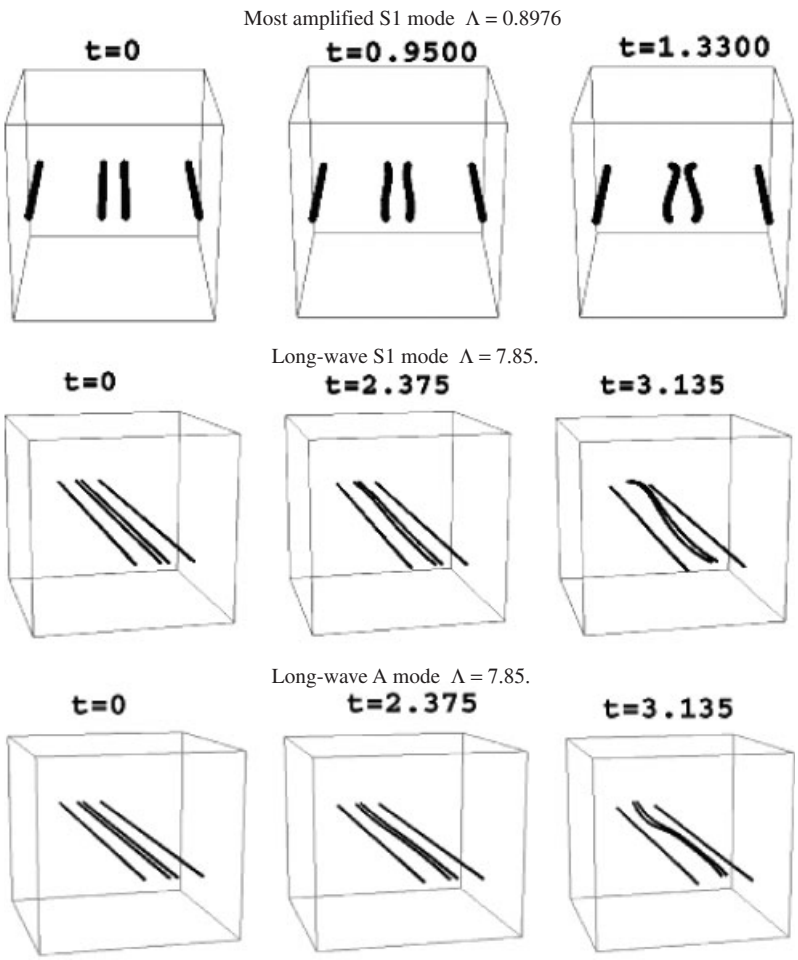

Figure 13. Vortex filament simulation of the non-linear instability regime of typical modes for the four-vortex wake. Initial amplitude $\rho_0 = 0.001$ and initial thickness $\varepsilon = 0.1$. (The visualization of the filaments uses equal core radius even if the computation uses unequal sizes.

7. CONCLUSION

A code EZ-vortex has been developed to compute the motion of slender vortex filaments of closed or open shape. The implemented equation is the M1 de-singularized method of Knio and Klein but other equivalent equations are also implemented as a useful comparison. The fluid may be inviscid or not, the vortex core is similar or not, and there can be an axial flow or not. The validity of all these equations are based on the Callegari and Ting asymptotic results. The advantages of the different formulations and discretizations of the associated equations are discussed. The difference between the closed and open filament for the filament centreline storage has been explained.

The philosophy of EZ-Vortex code is to keep programs as simple as possible and to provide documentation both by way of a text and comments within the code itself. It is available through the world-wide web.

This code has been validated against known solutions of these equations and results of linear stability studies. We recall known analytical results for a vortex ring, a vortex ring pair and a perturbed straight filament. The comparisons between these results and the EZ-vortex simulations are excellent. We give the optimal values of the numerical parameters that give converged results with the code.

The linear and non-linear stages of a perturbed two-vortex wake and of a four-vortex wake model are then studied till the reconnection phase, which is outside the validity of the asymptotic analysis and of the associated integro-differential equations. In the linear phase the comparison with analytical stability results is also excellent.

This code may be used to study other non-stationary four-vortex wake configurations as the one studied in the linear regime by Crouch [28] or the non-linear stage of two rotating vortices of different circulations. The higher order asymptotic result obtained by Margerit [29] may be implemented in order to get higher order results, i.e. thicker vortex core, and to offer the possibility of a quantitative comparison with a direct numerical simulation of the Navier–Stokes equations. Simple reconnection models [7] may be also implemented to go through the reconnection phase.

ACKNOWLEDGEMENTS

This work, performed within the C-Wake project, was supported by the European Community in the frame of the fifth Framework Research Program under contract GRD1-1999-10332. The authors would like to thank Dr. D. Fabre for providing stability results for the four-vortex aircraft wake model, and O. M. Knio and R. Klein for providing their Fortran code with the implementation of their M1-desingularized method for a closed filament. We would like to underline the importance of the Callegari and Ting asymptotic result (first obtained by Ting in 1971) giving the equation of motion for the centreline of a vortex filament.

REFERENCES

1. Huenecke K. Vortex wakes from large aircraft—a challenge for industrial research. *AIAA Paper* 2000; 2000–2216.
2. Puckett EG. Vortex methods: an introduction and survey of selected research topics. In *Incompressible Computational Fluid Dynamics—Trends and Advances*. Nicolaides RA, Gunzburger MD (eds). Cambridge University Press: Cambridge, 1993; 335–407.
3. Batchelor G. *Introduction to Fluid Dynamics*. Cambridge University Press: Cambridge, 1967.
4. Saffman P. *Vortex Dynamics*. Cambridge University Press: Cambridge, 1992; 33–38, 208–215.

5. Ting L. Studies in the motion and decay of vortices. In *Proceedings of the Symposium on Aircraft Wake Turbulence*, Olsen J, Goldburg A, Rogers R (eds). Seattle: Washington, 1971; 11–39.
6. Callegari A, Ting L. Motion of a curved vortex filament with decaying vortical core and axial velocity. *SIAM Journal on Applied Mathematics* 1978; **35**(1):148–175.
7. Ting L, Klein R. *Viscous vortical flows, Lecture Notes in Physics*. Springer: Berlin, 1991.
8. Liu C, Tavantzis J, Ting L. Numerical studies of motion and decay of vortex filaments. *AIAA Journal* 1986; **24**(8):1290–1297.
9. Leonard A. Computing three-dimensional incompressible flows with vortex elements. *Annual Review of Fluid Mechanics* 1985; **17**:523–559.
10. Crow S. Stability theory for a pair of trailing vortices. *AIAA Journal* 1970; **8**:2172–2179.
11. Hama F. Progressive deformation of a curved vortex filament by its own induction. *Physics of Fluids* 1962; **5**:1156–1162.
12. Widnall S, Sullivan J. On the stability of vortex rings. *Proceedings of the Royal Society London A* 1973; **332**:335–353.
13. Widnall S, Bliss D, Zalay A. Theoretical and experimental study of the stability of a vortex pair. In *Proceedings of the Symposium on Aircraft Wake Turbulence*, Olsen J, Goldburg A, Rogers R (eds). Seattle: Washington, 1971; 305–338.
14. Widnall S. The structure and dynamics of vortex filaments. *Annual Review of Fluid Mechanics* 1975; **7**:141–165.
15. Moore D, Saffman P. The motion of a vortex filament with axial flow. *Philosophical Transactions of the Royal Society London Series A* 1972; **1226**(272):403–429.
16. Margerit D, Brancher J-P. Asymptotic Expansions of the Biot-Savart law for a slender vortex with core variation. *Journal of Engineering Mathematics* 2001; **40**(3):297–313.
17. Klein R, Knio O. Asymptotic vorticity structure and numerical simulation of slender vortex filaments. *Journal of Fluid Mechanics* 1995; **284**:257–321.
18. Knio O, Klein R. Improved thin-tube models for slender vortex simulations. *Journal of Computational Physics* 2000; **163**(1):68–82.
19. Margerit D. EZ-Vortex documentation: a slender vortex filament solver. *IMFT Report*, 2001.
20. Barkley D. A model for fast computer simulation of waves in excitable media. *Physica D* 1991; **49**:61–70.
21. Dowle M, Mantel RM, Barkley D. Fast simulations of waves in three-dimensional excitable media. *International Journal of Bifurcation and Chaos* 1997; **7**(11):2529–2545.
22. Liu C, Tavantzis J, Ting L. Numerical studies of motion of vortex filaments-Implementing the asymptotic analysis. *AIAA Paper* 1984; **84-1542**:1–11.
23. Margerit D, Brancher J-P. Motion and oscillations of a circular perturbed vortex ring. *Comptes Rendus des Seances de Academie des Sciences Paris, Série II b* 2000; **328**:1–6.
24. Weidman PD, Riley N. Vortex ring pairs: numerical simulation and experiment. *Journal of Fluid Mechanics* 1993; **257**:311–337.
25. Kelvin. Vibration of a columnar vortex. *Philosophical Magazine* 1880; **10**:152–165.
26. Rennich SC, Lele SK. A method for accelerating the destruction of aircraft wake vortices. *AIAA Paper* 1998; **98-0667**:1–11.
27. Fabre D, Jacquin L. Stability of a four-vortex aircraft wake model. *Physics of Fluids* 2000; **12**(10):2438–2443.
28. Crouch JD. Instability and transient growth for two trailing-vortex pairs. *Journal of Fluid Mechanics* 1997; **350**:311–330.
29. Margerit D. The complete first order expansion of a slender vortex ring. In *IUTAM Symposium on Dynamics of Slender Vortices,* Krause E, Gersten K (eds). Kluwer: Aachen, 1997; 45–54.

